



POLITECNICO
MILANO 1863

Study on Nonreciprocal Behavior in Time-Space Modulated Beams

Control of structural band-gaps via shunted piezoelectric patches

Tommaso Bocchietti 10740309
Konstantinos Georgoussis 10992540
(Luciano Sarri 11071336)

12/02/2025

Politecnico di Milano

Agenda

1. Introduction
2. Shunted piezoelectric patches
3. Experimental results
 - Space-Only modulation
 - Space-Time modulation
4. Nonreciprocal behavior
5. Conclusions

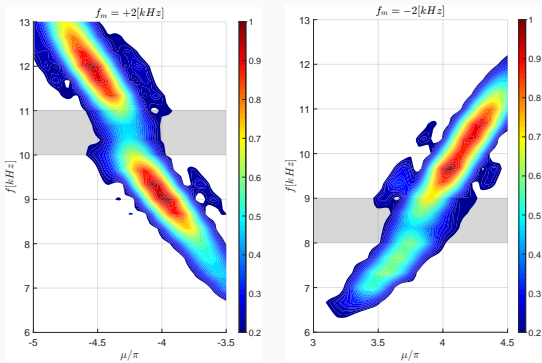


Figure 1: Experimental results of nonreciprocal behavior.

Introduction

Introduction to nonreciprocity

The principle of reciprocity states that in a linear time-invariant system (LTI), waves propagate from A to B in the same way as from B to A . The violation of this principle is referred to as **nonreciprocal** behavior.

One question arises: **is it possible to design a system that achieves nonreciprocal behavior?**

Experimental setup

The experimental setup¹ is composed of an array of shunted piezoelectric patches spaced 2 mm apart placed on an aluminum beam substrate. Toggling the switches that control the connection between the power supply and each negative capacitance shunting circuit, allows to modulate the substrate properties.

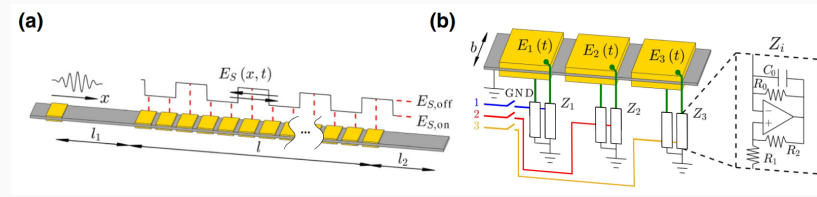


Figure 2: Beam substrate and array of piezoelectric patches (a), Spatio-Temporal cell and shunting circuits (b).

Out-of-plane velocity field is measured using a Polytec 3D laser Doppler vibrometer.

¹For numerical values and detailed description, refer to the attached project report (Section 4.1).

Experimental setup

By connecting the piezoelectric patches to the beam, the effective properties of the system are modified.

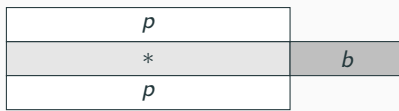


Figure 3: Connection between piezoelectric patches and beam.

$$\begin{aligned} EJ^* &= E_b J_b + 2E_p J_p \\ \rho A^* &= \rho_b A_b + 2\rho_p A_p \end{aligned} \quad (1)$$

Analysis of shunted piezoelectric patches

Piezoelectric patches sensitivity to RLC_N shunting circuit

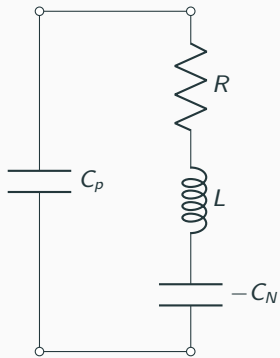


Figure 4: RLC_N shunting circuit

The mechanical admittance of piezoelectric patches is influenced by the presence of shunting circuits:

$$\begin{aligned} Y^{SU} &= Y_1^D \left(1 - \frac{k_{31}^2}{1 + sC_p^S Z^{SU}} \right) \\ &= Y_1^D \left(1 - \frac{k_{31}^2}{1 + C_p^S \left(-\frac{1}{C_N} - \omega^2 L \right) - sC_p^S R} \right) \end{aligned} \quad (2)$$

Negative capacitance ($-C_N < 0$) are active elements that can be implemented via OP-AMPS. As active elements, stability analysis is required:

- Mechanically stable if $Y^{SU} > 0$;
- Electrically stable if $C_{tot} > 0$.

A complete sensitivity analysis of $Y^{SU}(Z^{SU})$ is shown in the next slides.

Short vs. Open circuit case

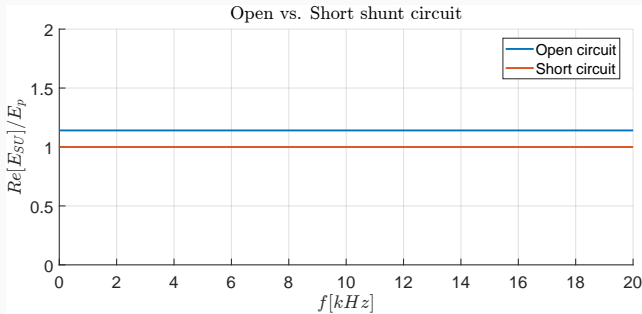


Figure 5: Analysis of Y^{SU} for the open and short circuit case.

As predicted by Equation 2, the piezoelectric patches' mechanical admittance in case of open circuit is greater than in case of short circuit. This causes a stiffer substrate and indeed a shift of the band-gap towards higher frequencies.

$$Y_1^D > Y_1^E = Y_1^D(1 - k_{31}^2) \quad (3)$$

Short vs. Open circuit case

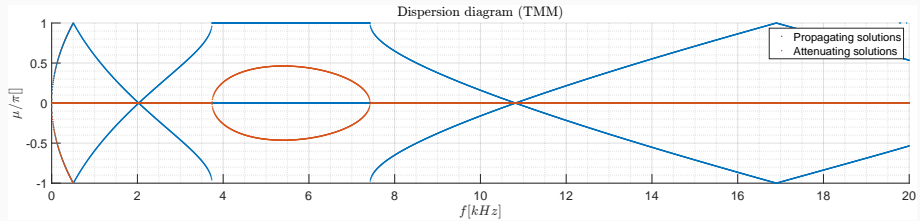


Figure 6: Short circuit case.

Short vs. Open circuit case

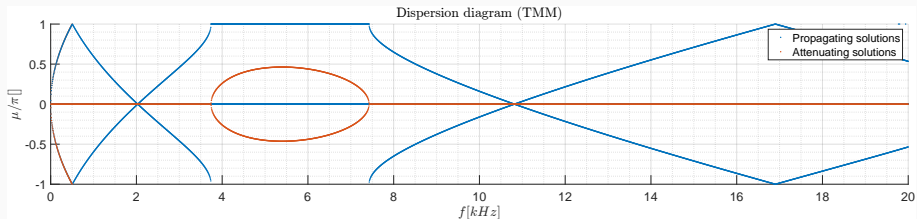


Figure 6: Short circuit case.

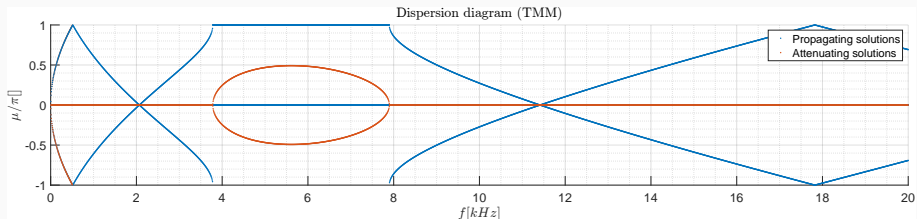


Figure 7: Open circuit case.

L shunt circuit

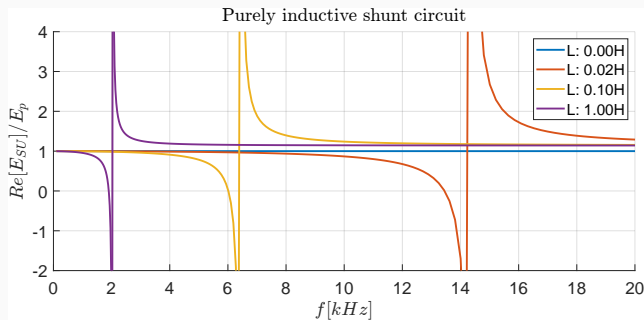


Figure 8: Analysis of Y^{SU} for the purely inductive shunt circuit.

In case of L shunt circuit, mechanical admittance of the piezoelectric patches is given by:

$$Y^{SU} = Y_1^D \left(1 - \frac{k_{31}^2}{1 - \omega^2 C_p^S L} \right) \quad (4)$$

Oscillatory behavior is expected around the natural frequency $\omega_n = \frac{1}{\sqrt{C_p^S L}}$.

L shunt circuit

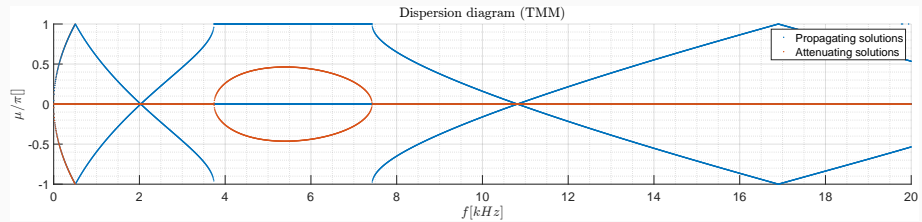


Figure 9: RLC shunt circuit with $R = 0\Omega$, $L = 0H$, and $C = \infty F$.

L shunt circuit

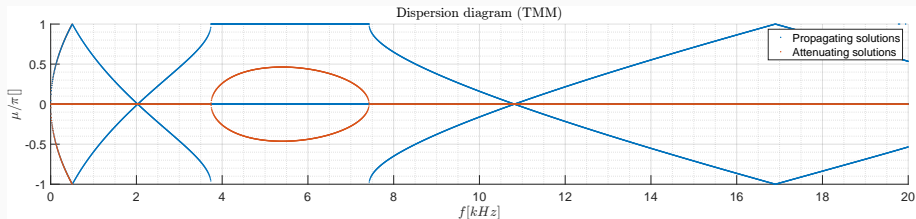


Figure 9: RLC shunt circuit with $R = 0\Omega$, $L = 0H$, and $C = \infty F$.

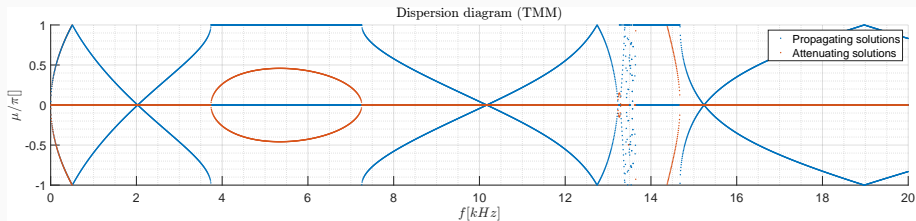


Figure 10: RLC shunt circuit with $R = 0\Omega$, $L = 0.02H$, and $C = \infty F$.

L shunt circuit

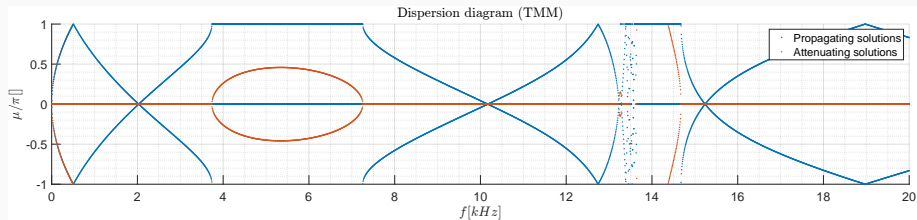


Figure 9: RLC shunt circuit with $R = 0\Omega$, $L = 0.02H$, and $C = \infty F$.

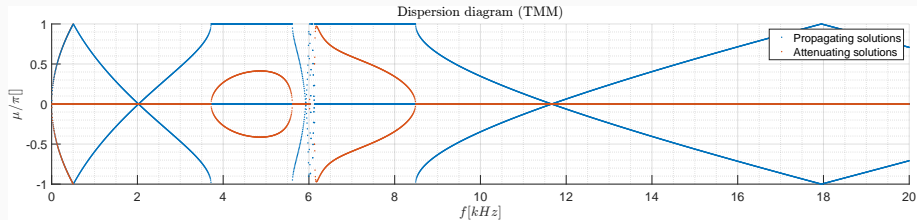


Figure 10: RLC shunt circuit with $R = 0\Omega$, $L = 0.10H$, and $C = \infty F$.

L shunt circuit

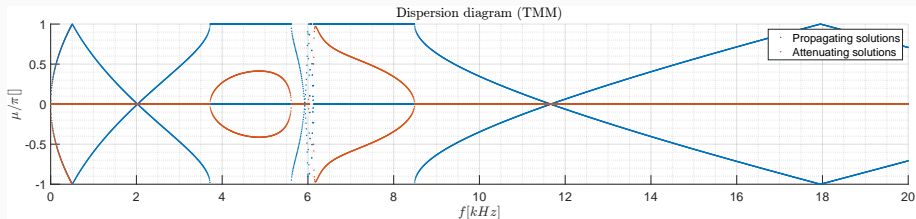


Figure 9: RLC shunt circuit with $R = 0\Omega$, $L = 0.10H$, and $C = \infty F$.

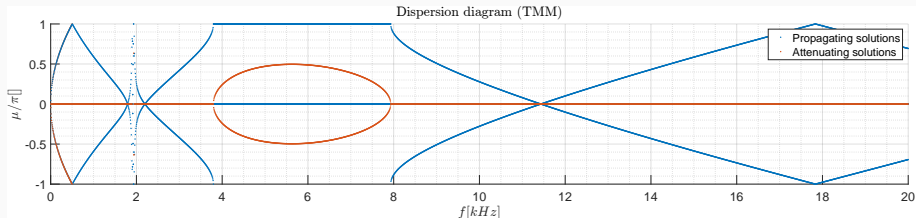


Figure 10: RLC shunt circuit with $R = 0\Omega$, $L = 1H$, and $C = \infty F$.

RL shunt circuit

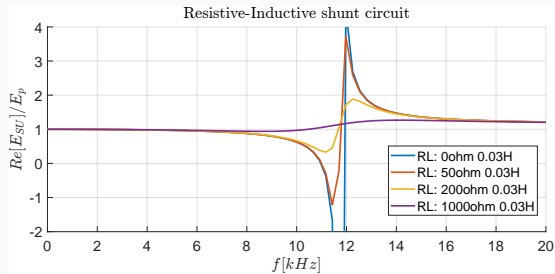


Figure 11: Analysis of γ^{SU} for the resistive-inductive shunt circuit.

In case of *RL* shunt circuit, mechanical admittance of the piezoelectric patches is given by:

$$\gamma^{SU} = \gamma_1^D \left(1 - \frac{k_{31}^2}{1 - \omega^2 C_p^S L - s C_p^S R} \right) \quad (5)$$

The resistive element R acts as a damping factor, controlling the width and depth of the band-gap. For high values of R , the band-gap can be completely suppressed.

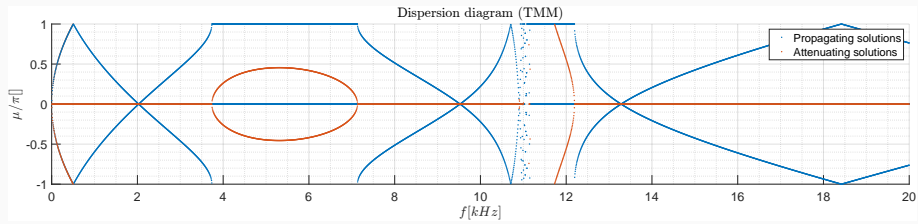


Figure 12: RLC shunt circuit with $R = 0\Omega$, $L = 0.03H$, and $C = \infty F$.

RL shunt circuit

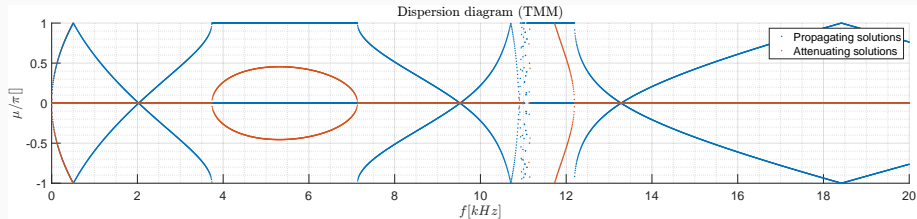


Figure 12: RLC shunt circuit with $R = 0\Omega$, $L = 0.03H$, and $C = \infty F$.

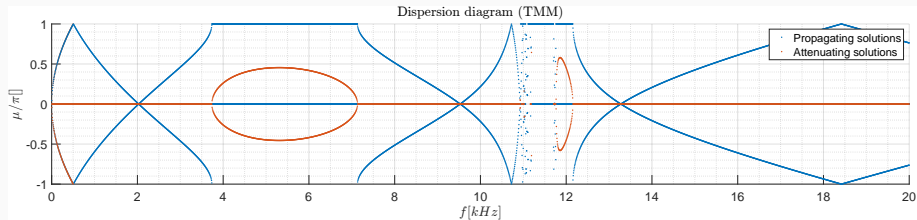


Figure 13: RLC shunt circuit with $R = 50\Omega$, $L = 0.03H$, and $C = \infty F$.

RL shunt circuit

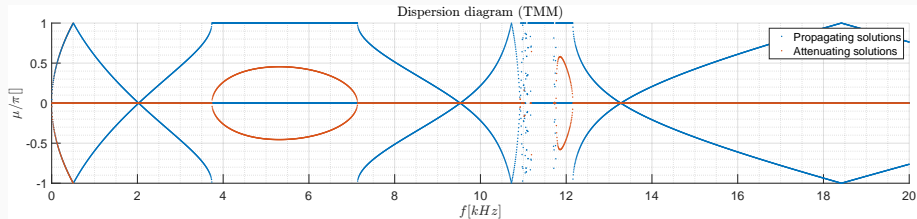


Figure 12: RLC shunt circuit with $R = 50\Omega$, $L = 0.03H$, and $C = \infty F$.

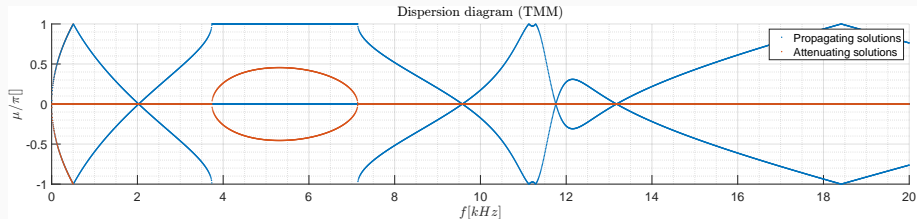


Figure 13: RLC shunt circuit with $R = 200\Omega$, $L = 0.03H$, and $C = \infty F$.

RL shunt circuit

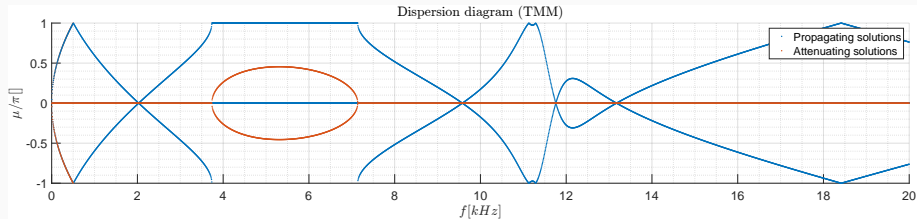


Figure 12: RLC shunt circuit with $R = 200\Omega$, $L = 0.03H$, and $C = \infty F$.

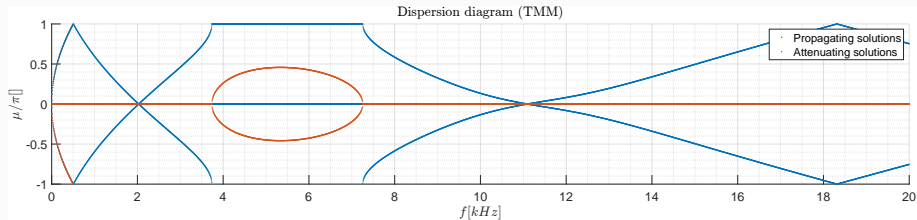


Figure 13: RLC shunt circuit with $R = 1000\Omega$, $L = 0.03H$, and $C = \infty F$.

RC_N shunt circuit

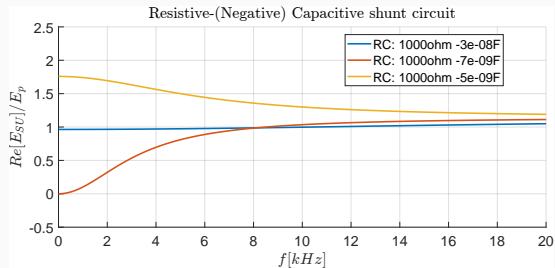


Figure 14: Analysis of Y^{SU} for the resistive-(negative) capacitive shunt circuit.

In case of RC_N shunt circuit, mechanical admittance of the piezoelectric patches is given by:

$$Y^{SU} = Y_1^D \left(1 - \frac{k_{31}^2}{1 - C_p^S \frac{1}{C_N} - sC_p^S R} \right) \quad (6)$$

The capacitative element has similar effects as the inductive one, with the ability to shift the band-gap toward lower or higher frequencies depending on the sign of $1 - C_p^S \frac{1}{C_N}$.

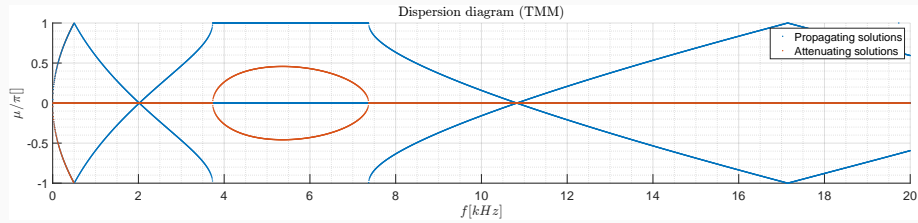


Figure 15: RLC shunt circuit with $R = 1000\Omega$, $L = 0H$, and $C = -30nF$.

RC_N shunt circuit

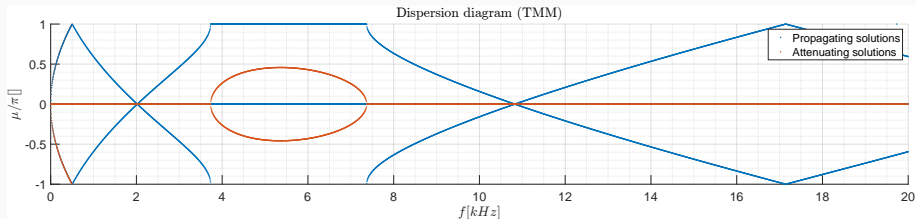


Figure 15: RLC shunt circuit with $R = 1000\Omega$, $L = 0H$, and $C = -30nF$.

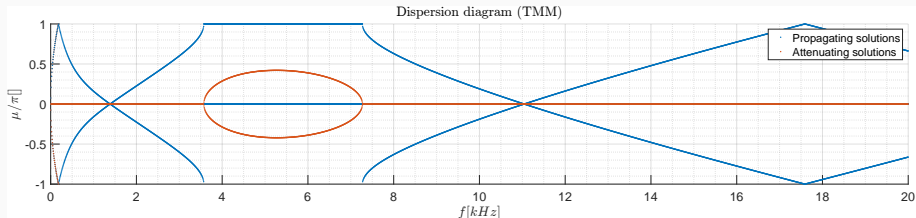


Figure 16: RLC shunt circuit with $R = 1000\Omega$, $L = 0H$, and $C = -7nF$.

RC_N shunt circuit

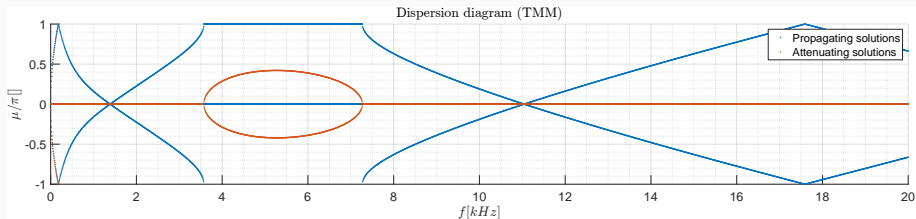


Figure 15: RLC shunt circuit with $R = 1000\Omega$, $L = 0H$, and $C = -7nF$.

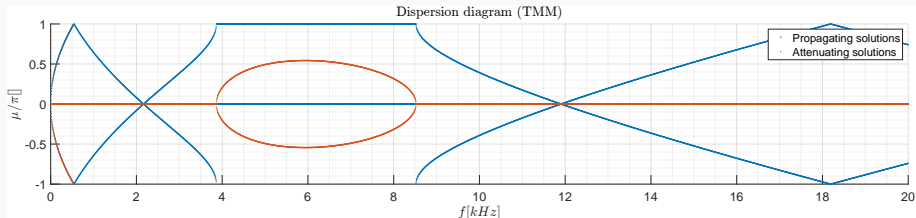


Figure 16: RLC shunt circuit with $R = 1000\Omega$, $L = 0H$, and $C = -5nF$.

Experimental results

Space-Only modulation

In the case of space-only modulation, piezoelectric patches can be either in the short-circuit (ON) or open-circuit (OFF) state. Three different configurations of the ST cell are considered:

- *OFF-OFF-OFF*
- *ON-ON-ON*
- *ON-OFF-OFF*

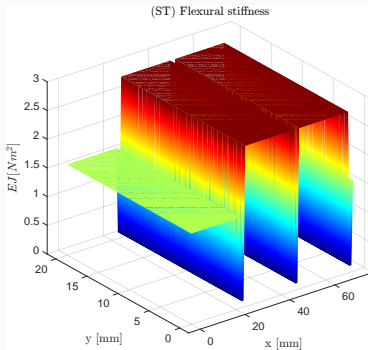


Figure 17: ST cell in the case *ON-OFF-OFF*.

Numerical simulations performed using TMM¹ and PWEM² are compared against experimental data. Comsol Multiphysics is also adopted as a valid reference.

¹Transfer Matrix Method

²Plane Wave Expansion Method

Case OFF-OFF-OFF

The first band-gap is observed at $f_{BG}^{OFF-OFF-OFF} = [3.8, 7.5] \text{kHz}$.

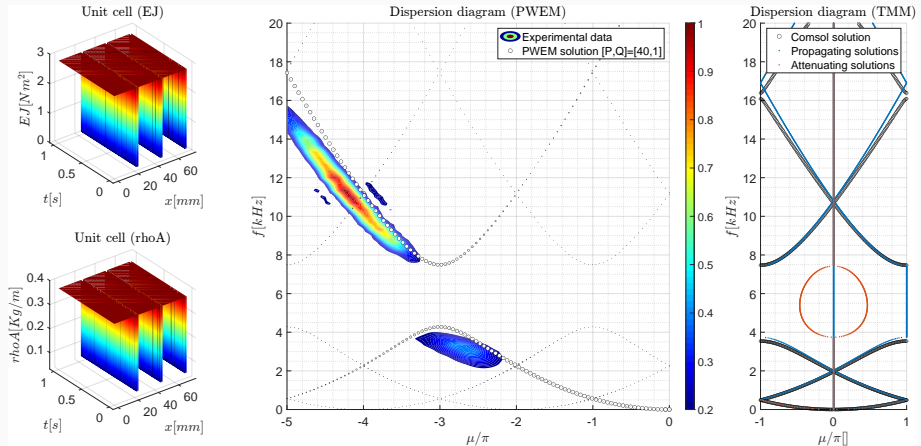


Figure 18: Dispersion diagram for the OFF-OFF-OFF configuration.

Case ON-ON-ON

Short-circuiting all the piezoelectric patches results in a decrease of the structural stiffness and a shift of the band-gap towards lower frequencies
 $(f_{BG}^{ON-ON-ON} = [3.4, 5.6] \text{kHz})$.

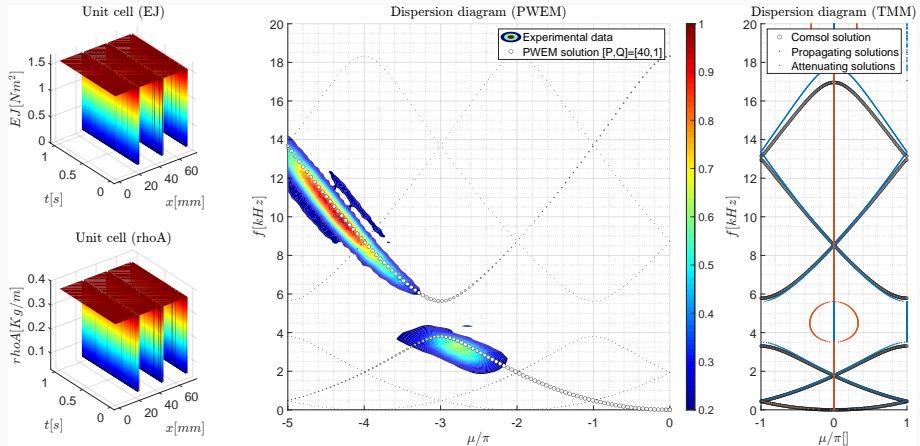


Figure 19: Dispersion diagram for the ON-ON-ON configuration.

Case ON-OFF-OFF

The introduction of additional sources of dispersion in the system results in a higher number of band-gaps visible in the same frequency range.

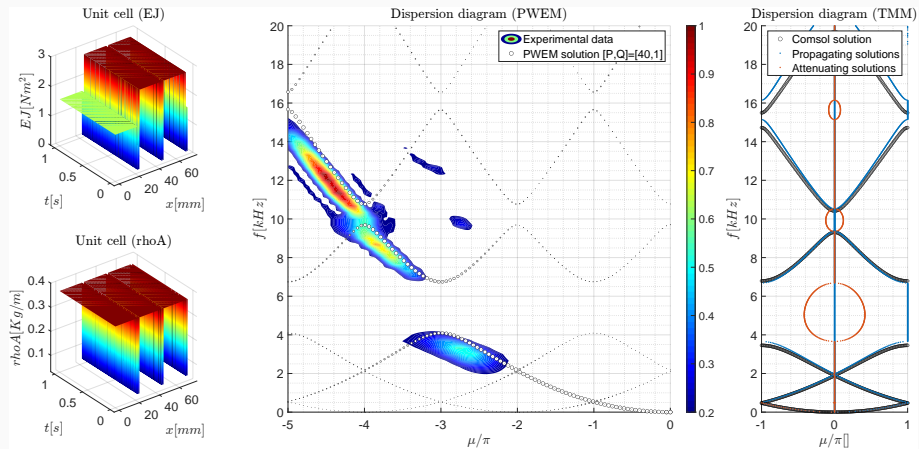


Figure 20: Dispersion diagram for the ON-OFF-OFF configuration.

For the case of space-time modulations, piezoelectric patches are driven by equal (but phase-shifted) signals. Three different pairs of shunt modulation frequencies ($\pm f_m$) are considered.

PWEM numerical simulations are compared against experimental data.

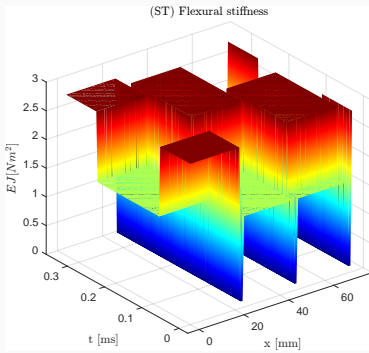


Figure 21: ST cell in the case $f_m = 3[\text{Khz}]$.

The mechanical admittance of the k -th piezoelectric patch in the ST cell is given by:

$$Y_k^{SU} = \frac{(Y^{OFF} + Y^{ON})}{2} + \frac{(Y^{OFF} - Y^{ON})}{2} \text{sign} \left[\cos \left(2\pi f_m t + (k-1) \frac{2\pi}{3} \right) \right] \quad (7)$$

Modulation $f_m = \pm 1\text{kHz}$

Time modulation causes anti-symmetric dispersion diagrams and directional band-gaps to appear. This is a clear indication of the nonreciprocal behavior of the structure.

A low frequency global band-gap is still present, associated with spatial modulation.

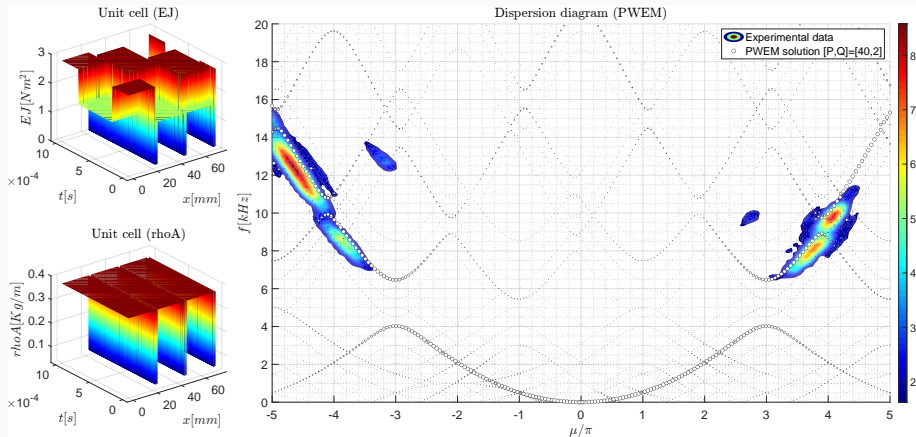


Figure 22: Dispersion diagram for the case of modulation frequency $f_m = \pm 1\text{kHz}$.

Modulation $f_m = \pm 2\text{kHz}$

Intuitively, the phenomenon associated with the nonreciprocal behavior is now more pronounced, as the modulation frequency is doubled. Band-gap associated with space modulation seems to remain unchanged.

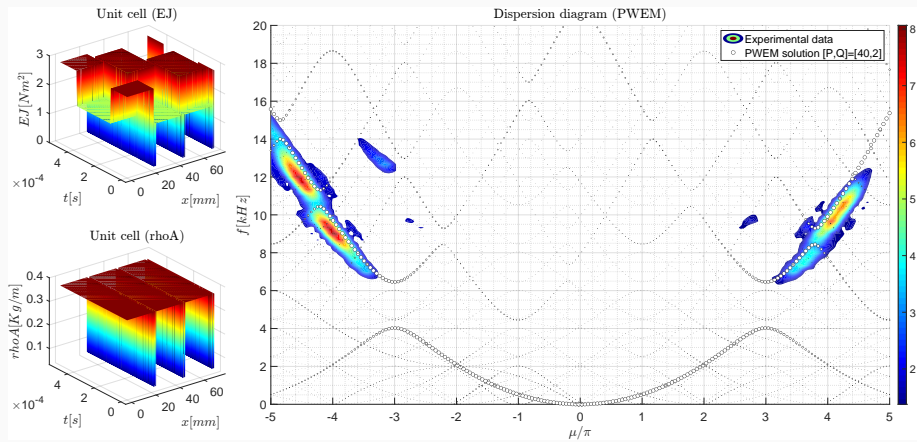


Figure 23: Dispersion diagram for the case of modulation frequency $f_m = \pm 2\text{kHz}$.

Modulation $f_m = \pm 3\text{kHz}$

The asymmetrical shift of the already previously analyzed directional band-gaps is even more evident. With respect to the case $f_m = 0\text{kHz}$ (*ON-OFF-OFF*), a total shift of around $\pm 1.5\text{kHz}$ has been observed in the directional band-gaps positions.

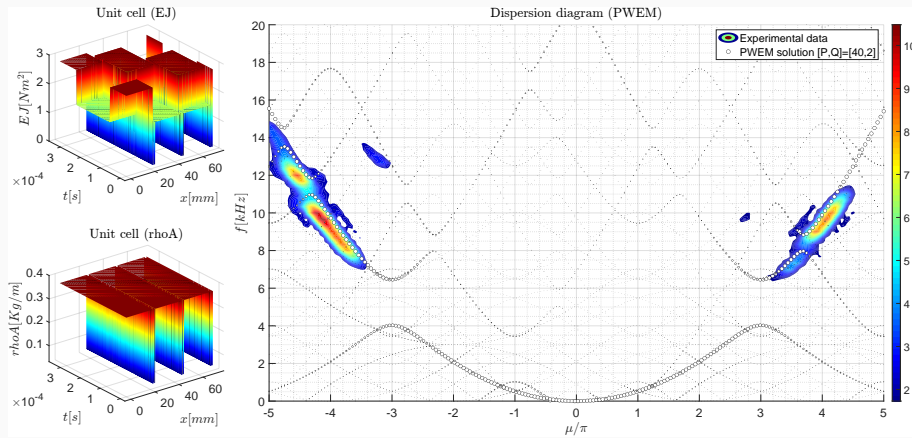


Figure 24: Dispersion diagram for the case of modulation frequency $f_m = \pm 3\text{kHz}$.

Nonreciprocal behavior

Performed tests

Both experimental and numerical simulations have shown that the structure exhibits a nonreciprocal behavior when excited with a time-space modulated signal.

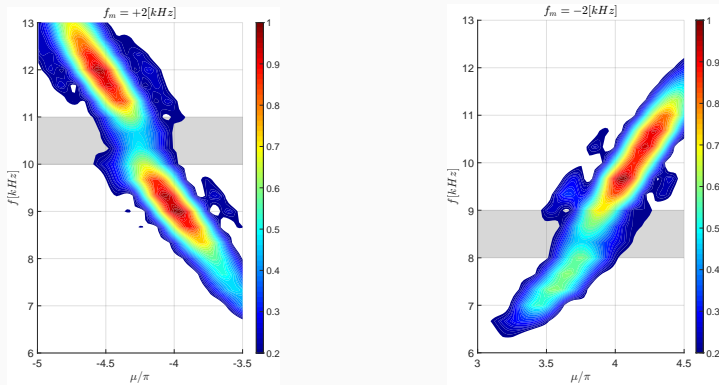


Figure 25: Experimental results for modulation frequency $f_m = \pm 2kHz$.

Two additional tests are performed using a narrow-band excitation signal at the two directional band-gaps frequencies already identified. Spectral analysis of the travelling waves is performed to further highlight nonreciprocity in the structure.

Spectral analysis

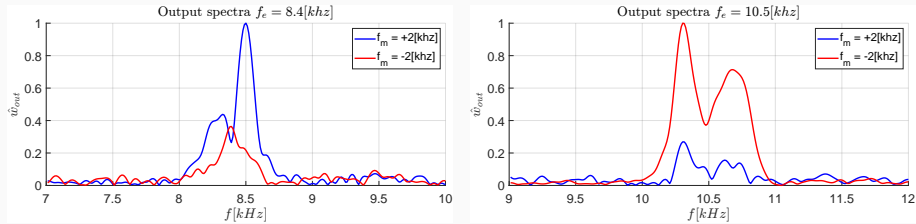


Figure 26: Spectral components of end-of-beam displacement for (left) $f_e = 8.4\text{kHz}$ and (right) $f_e = 10.5\text{kHz}$ excitations. Modulation frequency is set to $f_m = \pm 2\text{kHz}$.

Depending on the travelling direction considered, the wave propagates differently. The principle of reciprocity is therefore violated.

Conclusions

Summary of results

In this work we have shown that in a 1D beam structure, **nonreciprocal behavior can be achieved and controlled** by modulating its properties in time and space via shunted piezoelectric actuation.

The result is a diode-like behavior in the wave transmission, where the wave is allowed to propagate in one direction while being attenuated in the opposite direction if a directional band-gap is present.

The capability to control wave propagation in a nonreciprocal manner opens up a wide range of potential applications in the field of phononic devices and advanced signal processing, such as:

- Acoustic waveguides for unidirectional energy transfer;
- Enhanced vibration control systems in engineering structures;
- Phononic devices for advanced signal processing.

Future work may focus on refining the modulation strategies to achieve even greater control over wave propagation and exploring the scalability of this approach to other multidimensional structures such as plates and shells.

-  G. Cazzulani and G. Brambilla.
062239 - metamaterials and metastructures, 2024.
Lecture slides, Politecnico di Milano.
-  N. Hagood and A. von Flotow.
Damping of structural vibrations with piezoelectric materials and passive electrical networks.
Journal of Sound and Vibration, 146(2):243–268, 1991.
-  J. Marconi, E. Riva, M. Di Ronco, G. Cazzulani, F. Braghin, and M. Ruzzene.
Experimental observation of nonreciprocal band gaps in a space-time-modulated beam using a shunted piezoelectric array.
Phys. Rev. Appl., 13:031001, Mar 2020.
-  E. Riva, J. Marconi, G. Cazzulani, and F. Braghin.
Generalized plane wave expansion method for non-reciprocal discretely modulated waveguides.
Journal of Sound and Vibration, 449:172–181, 2019.

-  G. Trainiti and M. Ruzzene.
Non-reciprocal elastic wave propagation in spatiotemporal periodic structures.
New Journal of Physics, 18(8):083047, Aug. 2016.

Questions?

Thank you!